Di Giacomo, D., Grosser, H., Parolai, S., Bormann, P., Wang, R. (2008): Rapid determination of ME for strong to great shallow earthquakes. - Geophysical Research Letters, 35, L10308

DOI: 10.1029/2008GL033505.

Rapid determination of Me for strong to great shallow earthquakes

Domenico Di Giacomo[1,2], Helmut Grosser[1], Stefano Parolai[1], Peter Bormann[1], and Rongjiang Wang[1]

1) GeoForschungsZentrum Potsdam, Telegrafenberg, 14473 Potsdam, Germany

2) Institute of Geosciences, Universität Potsdam, Karl-Liebknecht-Strasse, 14476 Potsdam, Germany

Abstract

We propose a new rapid procedure for determining the energy magnitude Me for shallow events from broadband teleseismic P-wave signals within the distance range 20°-98°. To accomplish this task, we compute spectral amplitude decay functions for different periods using numerical simulations based on the reference Earth model AK135Q. By means of these functions, we correct the spectra of the teleseismic recordings for the propagation path effects, and calculate the radiated seismic energy E_S, and hence Me. We use cumulative P-wave windows for simulating a real- or near real-time procedure and test it for 61 shallow earthquakes. The results show that our approach is able to provide a rapid and reliable Me determination within 7-15 minutes after the earthquake origin time, and is therefore suitable for implementation in rapid response systems.

1. Introduction

The event magnitude, as a measure of "earthquake size", is a parameter of fundamental importance for characterizing seismic events and it must be available in a short time after the earthquake origin time (OT) to evaluate its damage potential and to guide rapid response activities. Over the past decades many magnitude scales have been developed that often emphasize a specific feature of the earthquake process, and, consequently, have a different meaning. The energy magnitude Me is related to a well-defined physical parameter of the seismic source, i.e., the radiated seismic energy E_S. The energy radiated by an earthquake as seismic waves is concentrated around the corner frequency of the source spectrum and this makes Me more suitable than the moment magnitude Mw in describing the damage potential of earthquakes (Boatwright and Choy, 1986; Bormann et al., 2002; Choy and Kirby, 2004). Mw is related to the low-frequency asymptote of the

source spectrum and describes the overall tectonic effect of the seismic source, whereas Me is calculated over a larger frequency range of the source spectrum that is more related to frequencies of engineering interest.

Since Me is a better estimator of the shaking damage potential, a rapid and robust procedure suitable for implementation in rapid response systems to determine Me shortly after OT needs to be developed. In this study we describe a new procedure to determine Me for shallow earthquakes by using broadband teleseismic recordings of P-waves in the distance range 20°-98°. The correction for the wave propagation effects is performed by using spectral amplitude decay functions derived from numerical simulation of Green's functions, and Me is computed for cumulative P-wave windows up to the S-wave arrival. We show that our procedure is flexible and is able to rapidly and robustly determine Me even for great earthquakes, such as the 26 December, 2004 Sumatra earthquake. We analyzed 61 earthquakes (source parameters listed in Table I) in the Mw range 6.0-9.3 using recordings of broadband stations managed by global networks (GEOFON, IRIS, GEOSCOPE), as well as regional networks. Finally, we compare our Me with the Me computed by the USGS and with the Mw determined by Harvard University.

2. Correction for the propagation effects

One of the most challenging aspects of the calculation of the energy radiated by a seismic source is the correction for the geometrical spreading and for frequency-dependent attenuation. Therefore, to calculate E_S from a seismogram, the energy loss experienced by the seismic waves during propagation must be recovered. For this purpose, we must compute spectral amplitude decay functions for different frequencies that can be applied to the whole Earth, since our procedure is intended to serve global seismic network centers. Therefore, the calculation of these functions has been performed by using the reference Earth model AK135Q (Kennett et al., 1995; Montagner and Kennett, 1996) and the Green's functions simulation code by Wang (1999). The advantage of using synthetic seismograms is the fact that, starting from a known point source function, we can account

for all propagation effects at different frequencies. We computed teleseismic (source depth 33 km) P-wave seismograms in increments of 1° in the distance range 20°-35°, and steps of 2.5° from 35° onwards. For the distance range 20°-35° we use denser spatial sampling because P-waves observed in this range are strongly affected by the significant variations in velocity and attenuation in the upper mantle and transition zone. The use of stations between 20°-30° is empirically justified since no bias is introduced in our final Me determination including stations in this distance range, but at the same time we can launch earlier our procedure. From the simulated time series the amplitude decay functions have been derived as follows: for each simulated distance, the Fourier spectra of the P-wave trains have been computed and, then, the spectral amplitude decay at each distance at a given period has been extracted. We also investigated the influence on the amplitude decay functions of different phases (like PP) arriving between the first P and S wave arrivals, but no significant changes in the functions have been observed.

In order to assess the influence of the source mechanism used to generate the synthetic waveforms, we simulated, for each distance, a set of time series resulting from many combinations of focal parameters, and computed the median, the 25^{th} and the 75^{th} percentile of the amplitude decay functions at each distance. The frequency dependence of the amplitude decay functions in Fig. 1 is highlighted by plotting them for periods between 1 s and 16 s in increments of one octave (Duda and Yanovskaya, 1993). As expected, Fig. 1 clearly shows that the amplitude decay is higher for shorter periods, and that the difference between the functions for longer periods gets progressively smaller, with the percentile ranges for 8 s and 16 s already overlapping.

In practice, to correct the velocity spectra recorded at the seismic stations, we use the median amplitude decay functions for periods between 1 s and 60 s in steps of 1/3 of one octave, so that an adequate number of frequencies is available when the integration of the corrected power velocity spectra is executed. To average out the source radiation pattern, we use seismic stations which assure a good azimuthal coverage around the source. The correction is truncated at 1 s since the Q model was obtained from data in the significant period between 1 - 3000 s only (Montagner

and Kennett, 1966). For shorter periods the decay functions are not reliable. This lower limit in the integration means that, at the present time, our procedure is applicable to earthquakes with a magnitude greater than about 5.8-6, but it does not limit our energy determination, since strong to great earthquakes have corner frequencies falling inside the frequency band where the correction is applied. Moreover, a detailed analysis of the data set at hand showed that above 1 Hz the signal-to-noise ratio (SNR) is very poor, limiting the use of such high frequencies.

3. E_S and Me determination

The energy released as elastic waves is proportional to the square of the ground motion velocity. Assuming a point source and averaging over a spherical surface around the source, E_S can be calculated from the vertical component of teleseismic P-wave records as follows:

$$E_S = \left[\frac{1}{15\pi\rho\alpha^5} + \frac{1}{10\pi\rho\beta^5}\right]\int_{f1}^{f2}\left|\frac{\dot{u}(f)}{G(f)/2\pi f}\right|^2 df\ ,$$

where α, β, and ρ represent the P-wave velocity, the S-wave velocity and the density at the seismic source, respectively, *f1* and *f2* are the minimum and the maximum cutoff frequencies of the integration, $\dot{u}(f)$ represents the P-wave velocity spectrum, $G(f)$ the Green's functions spectrum and f the frequency (Haskell, 1964; Purcaru and Berckhemer, 1978; Boatwright and Choy, 1986; Venkataraman and Kanamori, 2004). Once E_S has been calculated, Me is obtained from the relationship (e.g. Bormann et al., 2002):

$$Me = 2/3(\log_{10} E_S - 4.4), \text{ with } E_S \text{ given in Joule.}$$

To make our procedure suitable for implementation in rapid response systems and to take into account the effect of the rupture duration, we compute E_S and Me starting with a 4 s window length after the first P-wave arrival, and increasing it continuously until the S-wave arrival (time-variable cumulative energy windows), which resembles the cumulative body-wave magnitude of Bormann and Wylegalla (2005). Fig. 2 illustrates how our procedure works. For this event of Mw 6.5 (# 17 in Table I) a stable E_S determination is obtained about 30 s after the P-wave onset. This

time window would be long enough to cover the entire rupture duration. Therefore, a longer time window would not significantly increase the calculated E_S value. This also means that our Me determination can be obtained before the S-wave arrival if the rupture duration is shorter than the S-P time window. At best reliable Me determinations can be available about 7 min after OT using stations between 20° and 30°. This is not the case for extremely large earthquakes, such as the recent 26 December, 2004 Sumatra earthquake, for which the rupture duration was about 500 s (Ni et al., 2005). But even in such an extreme case our procedure could have yielded a stable Me already some 15 min after OT (Fig. 3), because the major energy release occurred within the first 250 s of the rupture process (Choy and Boatwright, 2007). Therefore, our result is in good agreement with the final Me determination by the USGS (see black diamond in Fig. 4).

As final Me values for the earthquakes listed in Table I, we take the average of the single station Me determinations. We used recordings with SNR ≥ 3 in the frequency band of our interest. Fig. 4 shows the comparison of our Me values ±1 standard deviation with the Me computed by the USGS, and with the Mw from Harvard University. Both Me(USGS) and Mw(HRV) determinations have been retrieved from the SOPAR database (http://neic.usgs.gov/neis/sopar/). The discrepancies between Me(GFZ) and Me(USGS) are relatively small, although Me(GFZ) is on average 0.17 magnitude units (m.u.) larger than Me(USGS) for Me < 8. This may be due to the use of different attenuation corrections or corrections for specific focal mechanism, which have been applied to the final Me(USGS) values but not to our data. Further, the S-P time window used in our analysis is long compared with the rupture duration for Me < 8. The overestimation ranges from being negligible to 0.2 m.u. in the worst case scenario (Choy and Boatwright, 2007). Nevertheless, our Me is sufficiently accurate for rapid response purposes and a thorough investigation of the Me(GFZ)-Me(USGS) differences will be the subject of further studies. The comparison Me(GFZ)-Mw(HRV) shows that their difference can be up to about one m.u. This is due to the sensitivity of Me to changes in stress drop and related shifts in the corner period of the source spectrum. In contrast, Mw is based on the assumption of constant stress drop and thus a constant E_S/M_0 ratio.

Global events for different focal mechanisms, however, show stress drop variations of about three orders of magnitude (Choy and Boatwright, 1995; Bormann et al., 2002; Choy and Kirby, 2004). This highlights the need for determining both Me and Mw to better assess the hazard potential of an earthquake .

4. Conclusions

We present a rapid and robust procedure to calculate Me in a short time after OT using P-waves of teleseismic seismograms in the distance range 20°-98°. The correction for the propagation path effects is accomplished by applying spectral amplitude decay functions for different periods, that have been computed using numerical simulations of Green's functions based on the reference Earth model AK135Q. Our procedure avoids the problem of the time window saturation effect in magnitude determination (Bormann et al., 2007) and can be implemented in rapid response systems since it allows to properly determine Me within minutes of the first P-wave arrival, even for great earthquakes with very long rupture duration, such as the 26 December, 2004 Sumatra earthquake. We applied our procedure to 61 recent earthquakes and showed that our Me determinations agree on average reasonably well with the more formal and accurate but slower Me determined by the USGS. Some still existing discrepancies will be the subject of further studies. Finally, the comparison of Me(GFZ) with Mw(HRV) shows that these two magnitude scales, as measures of two different aspects of the seismic source, should be used together to better evaluate the tsunami and the shaking potential of strong and great earthquakes.

Acknowledgments

This paper is part of the EU-SAFER project, contract number 036935. We thank J. Saul, K. Klinge, and S. Sandberg for the data set preparation, D. Bindi for useful discussions, and two anonymous reviewers for their valuable comments. K. Fleming kindly improved our English.

References

Boatwright, J., and G. L. Choy (1986), Teleseismic estimates of the radiated energy by shallow earthquakes, *J. Geophys. Res. 91*, B2, 2095-2112.

Bormann, P., M. Baumbach, G. Bock, H. Grosser, G. L. Choy, and J. Boatwright (2002), Seismic sources and source parameters, in *IASPEI New Manual of Seismological Observatory Practice*, P. Bormann (Editor), Vol. 1, GeoForschungsZentrum, Potsdam, Chapter 3, 1-94.

Bormann, P., and K. Wylegalla (2005), Quick Estimator of the Size of Great Earthquakes, *EOS Trans. AGU 86(46)*, 464.

Bormann, P., R. Liu, X. Ren, R. Gutdeutsch, D. Kaiser, and S. Castellaro (2007), Chinese National Network magnitudes, their relation to NEIC Magnitudes, and recommendations for new IASPEI magnitude standards, *Bull. Seism. Soc. Am. 97*, 114-127, doi:10.1785/0120060078.

Choy, G. L, and J. Boatwright (1995), Global patterns of radiated seismic energy and apparent stress, *J. Geophys. Res. 100*, B9, 18,205-18,228.

Choy, G. L., and S. Kirby (2004), Apparent stress, fault maturity and seismic hazard for normal-fault earthquakes at subduction zones, *Geophys. J. Int. 159*, 991-1012.

Choy, G. L, and J. Boatwright (2007), The energy radiated by the 26 December 2004 Sumatra-Andaman earthquake estimated from 10-minute P-wave windows, *Bull. Seism. Soc. Am. 97(1)*, S18-S24.

Duda, S. J., and T. B. Yanovskaya (1993), Spectral amplitude-distance curves for P-waves: effects of velocity and Q-distribution, *Tectonophysics 217*, 255-265.

Haskell, N. (1964), Total energy and energy spectral density of elastic wave radiation from propagating faults, *Bull. Seism. Soc. Am. 56(6)*, 1811-1842.

Kennett, B. L. N., E. R. Engdahl, and R. Buland (1995), Constraints on seismic velocities in the Earth from traveltimes, *Geophys. J. Int. 122*, 108-124.

Montagner, J.-P., and B. L. N. Kennett (1996), How to reconcile body-wave and normal-mode reference Earth models?, *Geophys. J. Int. 125*, 229-248.

Ni, S., H. Kanamori, and D. Helmberger (2005), Energy radiation from the Sumatra earthquake, *Nature 434*, 582.

Purcaru G., and H. Berckhemer (1978), A magnitude scale for very large earthquakes, *Tectonophysics 49*, 189-198.

Venkataraman, A., and H. Kanamori (2004), Effect of directivity on estimates of radiated seismic energy, *J. Geophys. Res. 109*, B04301, doi:10.1029/2003JB002548.

Wang, R. (1999), A simple orthonormalization method for stable and efficient computation of Green's functions, *Bull. Seism. Soc. Am. 89(3)*, 733-741.

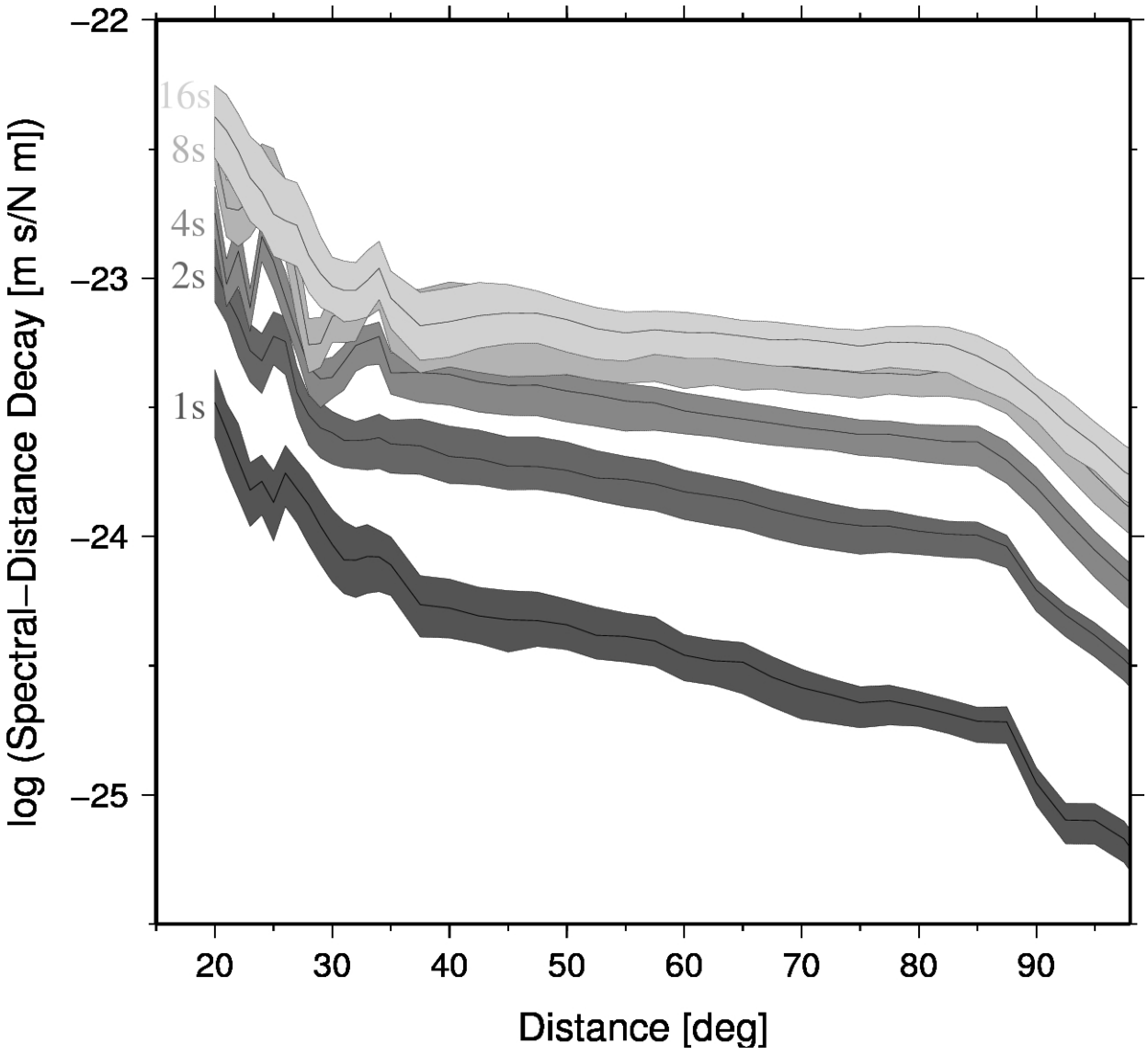

Fig. 1. Spectral amplitude decay functions for periods between 1 s and 16 s in steps of one octave. The solid lines represent the median spectral amplitude decay function for a given period, the shaded area represent the 25th and 75th percentile.

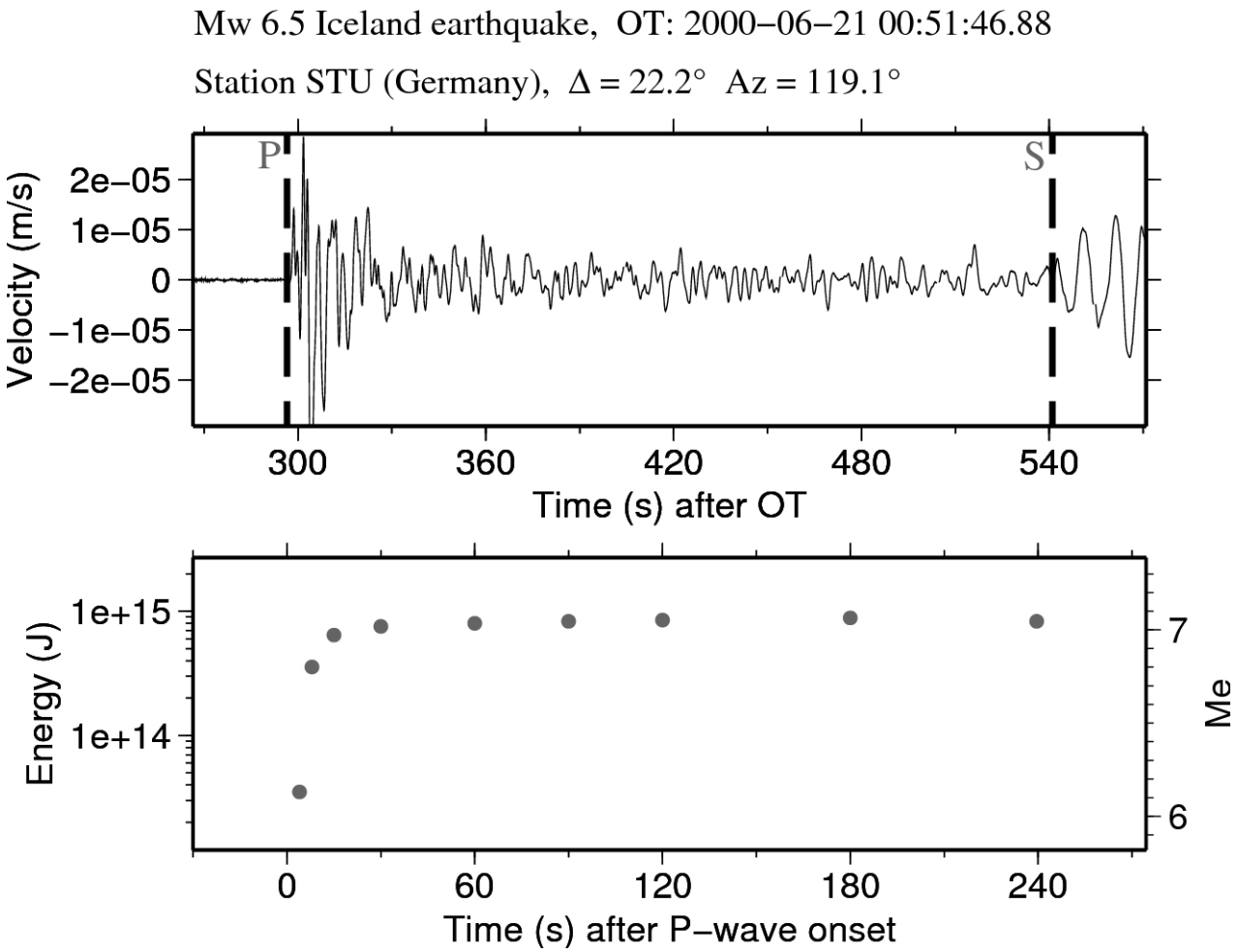

Fig. 2. Example describing how the procedure followed in this work is carried out. The upper panel shows the vertical component velocity recording of an Mw 6.5 Iceland earthquake (event # 17 in Table I) recorded at the station STU. The theoretical P- and S-wave arrival times have been marked by vertical broken lines. The lower panel shows the Energy and Me values for different cumulative P-waves windows.

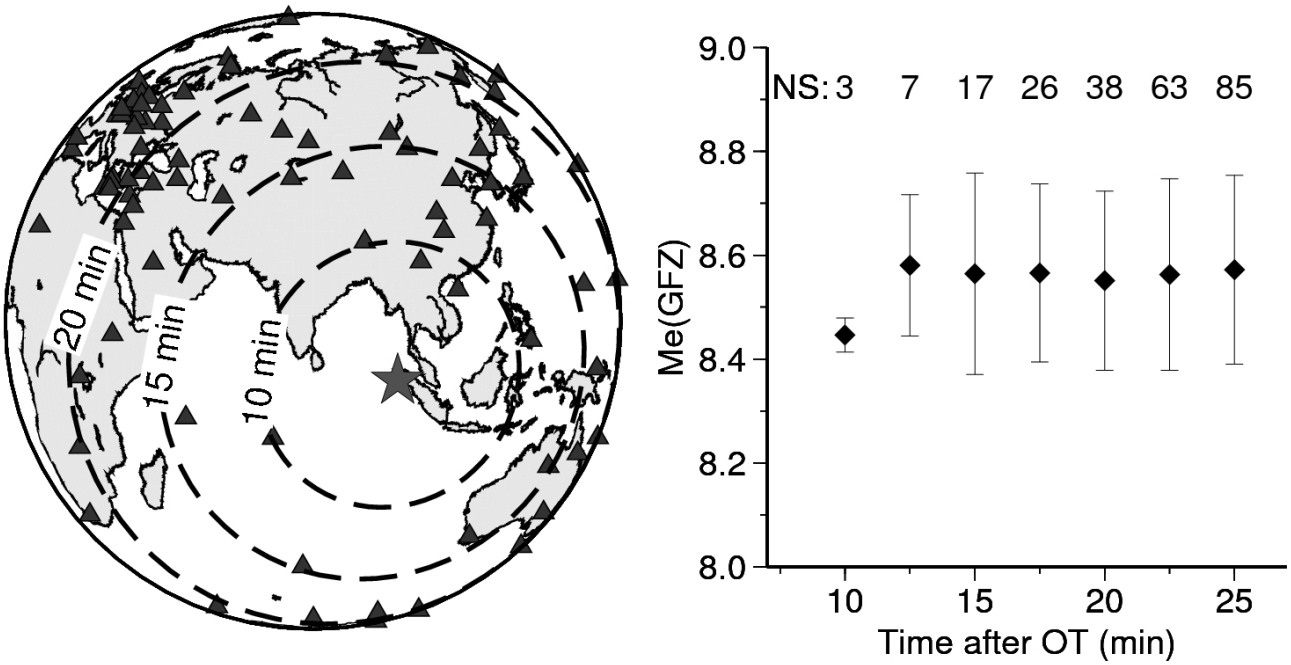

Fig. 3. Left: Map showing the location of the 26 December 2004 Sumatra earthquake (grey star), the broadband stations used to calculate Me (black triangles), and the dashed circles represent the S-wave arrival after OT. Right: Me(GFZ) determination of the Sumatra earthquake at different time after OT. The number of stations (NS) used to compute Me(GFZ) is also shown.

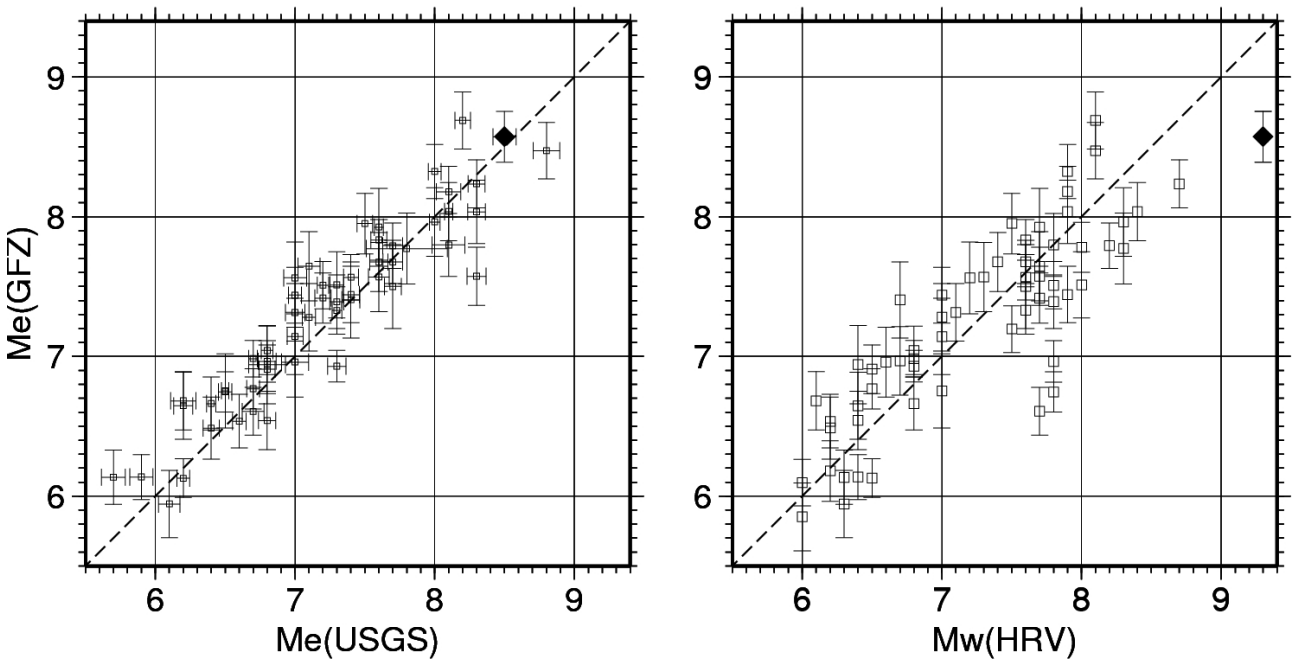

Fig. 4. Left: Comparison of Me(GFZ) and Me(USGS) estimates for the events listed in Table I, without the events # 6, 8, 18, 41 and 45 for which Me(USGS) is not available. The average Me values ±1 standard deviation are plotted. Right: Comparison of Me(GFZ) and Mw(HRV) estimates for all earthquakes listed in Table I. The black diamond represents the 26 December 2004 Sumatra earthquake.

Table I. List of earthquake parameters for the events analyzed in this work.

#	DATE	TIME	LAT	LON	DEPTH	Mw(HRV)	REGION	Me(GFZ)	Me(USGS)
1	1992-09-02	00:16:02	11.74	-87.34	44	7.7	Nicaragua	6.61±0.171	6.7±0.078
2	1994-06-02	18:17:34	-10.48	112.84	18	7.8	Java	6.75±0.143	6.5±0.048
3	1995-10-09	15:35:54	19.06	-104.21	33	8.0	Mexico	7.51±0.236	7.3±0.048
4	1995-12-03	18:01:09	44.66	149.30	33	7.9	Kuril Islands	7.44±0.201	7.4±0.060
5	1996-02-17	05:59:31	-0.89	136.95	33	8.2	Irian-Jaya	7.79±0.161	7.7±0.072
6	1996-02-21	12:51:01	-9.59	-79.59	10	7.5	Peru	7.20±0.167	na
7	1998-02-16	23:53:20	52.72	-33.68	10	6.8	North Atlantic Ridge	6.93±0.113	7.3±0.066
8	1998-03-20	21:08:09	-50.01	163.11	10	6.7	Auckland Islands Region	6.97±0.245	na
9	1998-03-25	03:12:25	-62.88	149.53	34	8.1	Balleny Islands Region	8.47±0.202	8.8±0.097
10	1998-11-29	14:10:32	-2.07	124.89	33	7.7	Ceram Sea	7.57±0.208	8.3±0.068
11	1999-08-17	00:01:39	40.75	29.86	17	7.6	Turkey	7.50±0.301	7.7±0.061
12	1999-09-20	17:47:19	23.77	120.98	33	7.6	Taiwan	7.42±0.180	7.2±0.058
13	1999-11-12	16:57:20	40.76	31.16	19	7.2	Turkey	7.56±0.256	7.0±0.082
14	2000-06-04	16:28:26	-4.72	102.09	33	7.8	Southern Sumatra	8.03±0.227	8.3±0.064
15	2000-06-17	15:40:42	63.97	-20.49	14	6.5	Iceland	6.77±0.143	6.7±0.046
16	2000-06-18	14:44:13	-13.80	97.45	14	7.9	South Indian Ocean	8.32±0.194	8.0±0.046
17	2000-06-21	00:51:47	63.98	-20.76	14	6.5	Iceland	6.91±0.174	6.8±0.058
18	2000-11-16	04:54:57	-3.98	152.17	33	8.0	New Ireland Region	7.78±0.178	na
19	2000-11-16	07:42:17	-5.23	153.10	30	7.8	New Ireland Region	7.51±0.170	7.2±0.041
20	2000-11-17	21:01:56	-5.50	151.78	33	7.8	New Britain Region	6.96±0.149	6.8±0.064
21	2000-12-15	16:44:48	38.46	31.35	10	6.0	Turkey	7.14±0.273	7.0±0.057
22	2000-12-06	17:11:06	39.57	54.80	30	7.0	Turkmenistan	6.10±0.166	5.4±0.031
23	2001-01-26	03:16:41	23.42	70.23	16	7.6	Southern India	7.92±0.279	7.6±0.032
24	2001-06-23	20:33:14	-16.26	-73.64	33	8.4	Peru	8.04±0.208	8.1±0.030
25	2001-08-21	06:52:06	-36.96	-179.84	33	7.1	New Zealand	7.31±0.205	7.0±0.070
26	2001-10-08	18:14:26	52.59	160.32	27	6.5	Kamchatka	6.13±0.138	6.2±0.045
27	2001-11-14	09:26:10	35.95	90.54	37	7.8	Qinghai	7.80±0.226	8.1±0.118
28	2002-03-25	14:56:34	36.06	69.32	8	6.2	Hinduksh	6.68±0.210	6.2±0.090
29	2002-09-08	18:44:24	-3.30	142.95	13	7.6	New Guinea Region	7.68±0.154	7.7±0.070
30	2002-11-03	22:12:41	63.74	-147.69	10	7.9	Alaska	8.18±0.182	8.1±0.088
31	2003-05-21	18:44:20	36.96	3.63	12	6.8	Northern Algeria	7.04±0.174	6.8±0.043
32	2003-07-15	20:27:50	-2.56	68.30	10	7.5	Carlsberg Ridge	7.83±0.145	7.6±0.057
33	2003-09-25	19:50:06	41.81	143.91	27	8.3	Off Coast of Hokkaido	7.96±0.246	8.0±0.039
34	2003-09-27	11:33:25	50.04	87.81	16	7.2	SW Siberia	7.57±0.247	7.6±0.074
35	2003-10-01	01:03:25	50.21	87.82	10	6.7	SW Siberia	7.41±0.272	7.4±0.064
36	2003-11-17	06:43:07	51.15	178.65	33	7.7	Aleuten	7.39±0.192	7.3±0.050
37	2004-09-28	15:29:54	-52.52	28.02	10	6.4	South of Africa	6.94±0.280	6.8±0.132
38	2004-10-09	21:26:54	11.42	-86.67	35	6.9	Nicaragua	6.75±0.265	6.5±0.026
39	2004-11-08	15:55:01	24.10	122.54	29	6.3	Taiwan	6.13±0.194	5.7±0.086
40	2004-12-26	00:58:53	3.30	95.98	30	9.3	Sumatra	8.57±0.182	8.5±0.083
41	2005-02-05	04:03:14	2.26	94.99	30	6.0	Sumatra	5.85±0.243	na
42	2005-02-22	02:25:23	30.74	56.83	14	6.4	Iran	6.65±0.239	6.2±0.069
43	2005-03-20	01:53:42	33.81	130.13	10	6.6	Kyushu-Japan	6.96±0.251	7.0±0.097
44	2005-03-28	16:09:37	2.09	97.11	30	8.6	Sumatra	8.23±0.172	8.3±0.060
45	2005-04-02	12:52:37	78.61	6.10	11	6.2	Svalbard	6.18±0.217	na
46	2005-08-26	18:16:33	14.42	52.37	25	6.2	Gulf of Aden	6.49±0.222	6.4±0.058
47	2005-10-08	03:50:41	34.54	73.59	26	7.6	Pakistan	7.57±0.163	7.4±0.054

48	2005-12-05	12:19:55	-6.22	29.83	22	6.8	Tangyika Lake	6.66±0.190	6.4±0.034
49	2006-01-02	06:10:49	-60.93	-21.58	22	7.4	South Sandwich Islands	7.68±0.212	7.6±0.065
50	2006-01-04	08:32:32	28.16	-112.12	14	6.6	Gulf of California	6.54±0.192	6.6±0.048
51	2006-01-08	11:34:54	36.31	23.21	66	6.8	Southern Greece	6.98±0.132	6.7±0.030
52	2006-02-14	15:27:23	20.82	146.18	37	6.3	Mariana Islands	5.94±0.239	6.1±0.077
53	2006-02-22	22:19:08	-21.22	33.34	23	7.0	Mozambique	7.28±0.241	7.1±0.047
54	2006-04-20	23:25:02	60.95	167.09	22	7.6	Eastern Siberia	7.33±0.169	7.3±0.034
55	2006-05-26	22:53:59	-7.96	110.45	13	6.4	Java	6.54±0.209	6.8±0.061
56	2006-07-17	08:19:24	-9.22	107.32	34	7.7	Java	7.64±0.247	7.1±0.079
57	2006-11-15	11:14:16	46.68	153.22	28	8.3	Kuril Islands	7.77±0.253	7.8±0.290
58	2006-12-01	14:01:49	-8.22	118.78	24	6.4	Sumbawa	6.14±0.162	5.9±0.083
59	2006-12-26	12:26:25	21.87	120.66	10	7.0	Taiwan	7.44±0.200	7.0±0.046
60	2007-01-13	04:23:23	46.26	154.39	18	8.1	Kuril Islands	8.69±0.205	8.2±0.055
61	2007-01-21	11:27:45	1.06	126.28	22	7.5	Molucca Sea	7.95±0.217	7.5±0.056